

Frequency and Duration of Communication System Outages Resulting From Polarization Mode Dispersion

D. Yevick, *Fellow, IEEE*, M. Reimer, H. Yaffe, *Member, IEEE*, P. J. Leo, D. L. Peterson, *Senior Member, IEEE*, S. Wang, and K. B. Rochford, *Senior Member, IEEE*

Abstract—In this paper, we employ measurements of transponder tolerance to both differential group delay (DGD) and second-order polarization mode dispersion (SOPMD) and of the temporal evolution of DGD and SOPMD in installed transmission systems to predict the influence of PMD on the rate and duration of PMD-induced system outages. An empirical 2-D random-walk model predicts that the outage rate and duration depends solely on the mean fiber DGD. We find that the step size of the random walk is nearly uncorrelated with the instantaneous value of the PMD. We then justify the assumptions of this procedure with a full numerical simulation and employ a biased Markov chain algorithm to generate highly accurate results for system outages where simplified models fail.

Index Terms—Monte Carlo methods, numerical analysis, optical fiber applications, optical fiber polarization, polarization mode dispersion (PMD).

I. INTRODUCTION

POLARIZATION mode dispersion (PMD) complicates the assessment of network performance because of its time-varying nature. Estimates of PMD-induced outages are often quantified in minutes per year [1]. However, this metric does not provide insight into the frequency or duration of outage events. For example, if one claims an impairment of 53 min a year, does this occur as one yearly event, or a distribution of shorter events? This issue impacts both static point-to-point links, which can accommodate PMD outages with dedicated protection switching, and networks for which the total PMD from transmitter to receiver will depend on routing that normally changes with time. Accommodating the provision of various paths in a network may, therefore, ultimately require adaptive compensation for

PMD. However, accurate knowledge of the PMD impairments and dynamics for the possible paths are required in order to prescribe the optimum mitigation technique.

Recently, Caponi *et al.* measured time-dependent differential group delay (DGD) and then estimated the mean outage rate and duration in an embedded fiber with a mean DGD, $\langle \tau \rangle = 9.4$ ps [2]. This analysis was based on the absence of correlation between the Maxwellian probability distribution of the DGD and the probability distribution of DGD change (expressed below in units of ps per hour). Consequently, an analytic 1-D level crossing model could be applied to determine the mean outage rate [3], [4]. However, PMD system outages are not exclusively influenced by DGD as receivers are also sensitive to distortions induced by the frequency variation of PMD associated with the magnitude of the frequency derivative of the polarization mode dispersion vector, i.e., the second-order PMD (SOPMD).

In this paper, we accordingly extend Caponi's model to address the simultaneous effects of both DGD and SOPMD on system outages. For a fiber with a known value of $\langle \tau \rangle$, the probability of an instantaneous state with a certain DGD and SOPMD is given by the 2-D joint probability density function (J-PDF) [5]. We here combine numerical techniques with temporal measurements of DGD and SOPMD taken on an installed buried fiber to simulate the evolution of instantaneous PMD states over the J-PDF with time. To model this evolution accurately, however, we must determine not only the PMD behavior of the fiber, but also the PMD tolerance of the transponder. Therefore, we measured a commercial transceiver's tolerance to DGD and SOPMD with a programmable PMD source, and employed this data to determine the combinations of DGD and SOPMD that give rise to the excessive penalties associated with system outages. Superimposing these penalties on the J-PDF yields an "outage boundary" that separates PMD states with acceptable penalties from those with excessive outage inducing penalties. We then simulate DGD/SOPMD evolution and monitor the crossings of this outage boundary in order to gather statistics on the occurrences and durations of PMD-induced outage events. The distributions of times between outages provide important information for protected links for which the frequency of outages has far greater practical relevance than their duration.

Further, we present a simplified alternative model of PMD time evolution based on the stochastic variation of mode-coupling angles in a standard fiber emulator. We demonstrate that this numerical model of PMD evolution yields a PMD step-size

Manuscript received September 12, 2007; revised February 1, 2008. Published August 29, 2008 (projected). This work was supported by the Natural Sciences and Engineering Research Council of Canada (NSERC).

D. Yevick and M. Reimer are with the University of Waterloo, Waterloo, ON N2L 3G1, Canada (e-mail: yevick@uwaterloo.ca).

H. Yaffe is with New Ridge Technologies, Reisterstown, MD 21136 USA (e-mail: hyaffe@newridgetech.com).

P. J. Leo is with the Diamantina Institute for Cancer, Immunology and Metabolic Medicine, University of Queensland, Brisbane, Qld. 4072, Australia (e-mail: pleo@cicr.uq.edu.au).

D. L. Peterson is with Verizon Business, Richardson, TX 75082 USA (e-mail: danny.peterson@verizonbusiness.com).

S. Wang is with Mintera Corporation, Acton, MA 01720 USA (e-mail: tony.wang@mintera.com).

K. B. Rochford is with NIST Optoelectronics Division, Boulder, CO 80305-3328 USA (e-mail: rochford@boulder.nist.gov).

Digital Object Identifier 10.1109/JLT.2008.922184

distribution consistent with experimental measurements, further justifying the assumptions of the empirical random-walk model of the preceding paragraph. It is of fundamental importance to note, however, that our model unlike that of [4] is based on local rather than global fiber parameters. Therefore, it can immediately be applied to general fiber links in which the birefringence of individual sections of an optical fiber vary stochastically but at different rates according to the particular properties of the local environment. On the other hand, in the simplified implementation of this paper, we vary each mode-coupling angle of the fiber emulator stochastically but with identical magnitude distributions, so that an experimental PMD time series can be characterized with a single measurement of the fiber's drift time [6]. Our results then apply principally to systems for which the properties of the outage states are dominated by first-order PMD.

II. MEASUREMENT OF TRANSPONDER PMD TOLERANCE

In this section, we briefly describe our experimental technique, which will be applied to 10-Gb/s signals in fibers with $15 \text{ ps} \leq \langle \tau \rangle \leq 35 \text{ ps}$, corresponding to the range of states generated by our DGD source. In particular, we will characterize the PMD penalty of a commercial OC-192 transponder with a DGD- and SOPMD-programmable PMD source.

PMD-related system penalties can be determined from the noise-loaded bit error rate (BER) [7]. The BER is measured at several optical signal-to-noise ratios (OSNRs) by attenuating the 10-Gb/s nonreturn-to-zero (NRZ) OC-192 transmitter signal immediately before an optical amplifier. After the back-to-back characteristic of the transponder is recorded in the absence of PMD impairment, a programmable PMD generator is placed after the transmitter and a polarization scrambler [7].

In this study, we limit our characterization of a PMD state to the magnitude of its DGD and SOPMD, where the principal contribution to SOPMD results from the depolarization of the PMD vector with optical frequency while the polarization-dependent chromatic dispersion is negligible as noted in [1]. Our PMD generator provides a wide range of reproducible DGD and SOPMD combinations [8] with these desired properties. In this manner, we can locate the boundaries on the J-PDF beyond which transponder penalties result in transmission outages. Accurately characterizing the transponder tolerance to a particular PMD state may require many hours of testing, during which the PMD generator must maintain the desired state. In contrast, for PMD emulators that dynamically generate PMD states, the state in which a given penalty occurs is unknown and only an "average" penalty over all instantaneous PMD states is obtained.

With our PMD source, BER versus OSNR curves can be determined for various DGD and SOPMD combinations. The system penalty for each PMD state is defined as the increase in OSNR (compared to zero PMD penalty) required for a BER of 10^{-12} . We measured the OSNR penalty exhibited by commercial transponders at 89 different DGD and SOPMD states, with DGDs ranging from 0 to 80 ps, and SOPMDs from 0 to 2500 ps^2 . In general, the penalty of all transponders increases monotonically with the DGD; further, we have observed that the penalty of many commercial transponders varies similarly as a function of the SOPMD at a fixed DGD.

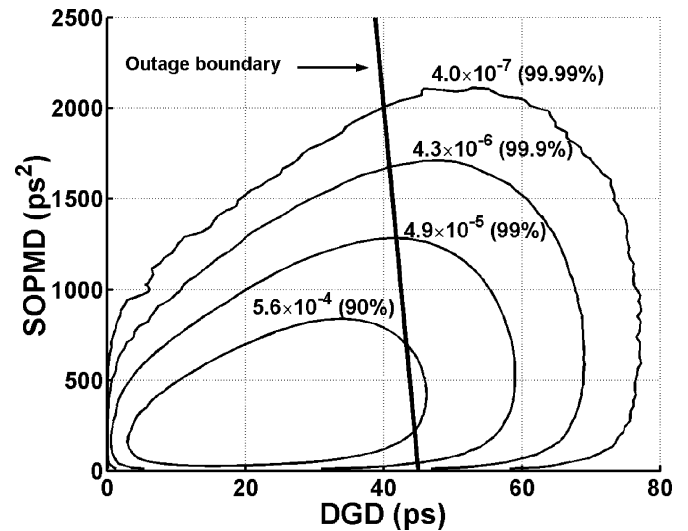


Fig. 1. J-PDF of the DGD and SOPMD for a $\langle \tau \rangle = 25 \text{ ps}$ fiber. The contours are labeled by the probability density followed in parentheses by the cumulative probability that the PMD state (DGD and SOPMD) will occur. For example, 90% of the time the PMD will lie within the inner contour labeled with probability density 5.6×10^{-4} . Also shown is an outage boundary for a commercial transponder.

The OSNR margins of optical communication systems are allotted to various parameters that degrade performance such as chromatic dispersion, self-phase modulation, and PMD. In our example, we assume that 3 dB of OSNR penalty is budgeted to PMD; that is, values of PMD that lead to penalties larger than 3 dB yield a system outage. Therefore, we measured the OSNR penalty at a large number of PMD generator states, for which the DGD was sampled at 5- or 10-ps intervals, while the SOPMD values were nominally separated by $\sim 200 \text{ ps}^2$. For our receiver measurements, the penalty approached 3 dB for the values of DGD = 45 ps and SOPMD = 0 ps^2 . With $\tau = 45 \text{ ps}$, we found that the penalty rose to 5 dB as the SOPMD was increased to 2500 ps^2 , while for comparison the penalty was about 3 dB for 40-ps DGD and 2000- ps^2 SOPMD. Accordingly, for this receiver, we can define an approximate outage boundary line rising from (45 ps, 0 ps^2) to (40 ps, 2000 ps^2). The outage boundary for this transponder is superimposed on the J-PDF for a $\langle \tau \rangle = 25 \text{ ps}$ fiber in Fig. 1. This boundary approximately separates states with penalties less than and greater than 3 dB, which are located to the left and right of the boundary, respectively. Since every transponder design has different DGD and SOPMD tolerances, the outage boundary is unique to this particular transponder and is employed only to illustrate our method [7].

III. DGD/SOPMD TIME-EVOLUTION MEASUREMENTS

We repeatedly measured the time variation of the first- and second-order PMD in a target fiber to obtain distributions of the rates of change of DGD and SOPMD. A typical temporal measurement examined the first span of a 3-span, 110-km direct-buried route [9], where two fibers from this span with $\langle \tau \rangle = 36 \text{ ps}$ were looped-back and connected to a tunable laser and commercial polarimeter to enable Jones matrix eigenanalysis

(JME) measurements at each wavelength [10]. Appropriate numerical derivatives calculated over pairs of wavelengths yielded the DGD and the SOPMD. A wavelength range of 20 nm was analyzed every 1.6 h over 174 h with 20-pm steps. The measurement was then repeated on another 36-ps fiber pair on the third span with similar results. By comparing these JME measurements against our stable programmable PMD generator [8], and noting the repeatability among field measurements taken within a few minutes at a fixed wavelength, we estimated that the uncertainty in our DGD and SOPMD values does not exceed 10%. Unlike the PMD tolerance analysis of Section II, however, our results are independent of the particular transponder implementation and unambiguously determine the time and wavelength variation of the fiber's DGD and SOPMD.

In order to model the temporal evolution of the PMD state, we require measurements over a time interval significantly larger than the correlation time associated with the PMD time evolution. However, it suffices to record many data sets over time intervals smaller than the correlation time, so that the amount of relevant data can be greatly increased by including data from different uncorrelated wavelength bands. In the frequency domain, PMD measurements separated by 24 GHz are essentially uncorrelated for a 36-ps fiber [11]. Thus, by analyzing the recorded time series at wavelengths separated by 24 GHz, we obtain numerous statistically independent ensembles, each of 174-h duration, that together provide an effective 4.73 years of temporal data taken at 1.6-h intervals.

A convenient estimate of the correlation time is provided by the wavelength-averaged temporal autocorrelation function (ACF) of the DGD and SOPMD time histories [6]

$$\begin{aligned} \rho_{xx}(k) &= \frac{1}{M(N-k)} \sum_{m=1}^M \sum_{n=1}^{N-k} x(n\Delta t, m\Delta\lambda)x((n+k)\Delta t, m\Delta\lambda). \end{aligned} \quad (1)$$

Here the N time samples are recorded at intervals Δt , while the M wavelength samples are separated by intervals $\Delta\lambda$. The term $x(t, \lambda)$ represents the magnitude of the DGD or the SOPMD. This temporal autocorrelation was applied to the full DGD vector in [11]; however, in [12], it was demonstrated that the above expression also holds for the magnitude of the DGD and the SOPMD.

Fig. 2 shows the normalized ACF for the DGD of one of the PMD impaired links examined in this study. The DGD has an average drift time of 1.3 days as defined by [11] with similar SOPMD behavior. Thus, in the time domain, measurements separated by less than 11 h are highly correlated since the ACF exceeds 0.89, while by 160 h the ACF has decreased to 0.1 indicating nearly uncorrelated PMD states (for visual clarity, the large time behavior of the ACF is not displayed in Fig. 2).

A central finding upon which we will base much of our computational formalism is that the magnitude of the change in the PMD state over one time step in properly normalized units is nearly uncorrelated with the instantaneous value of DGD and SOPMD. Accordingly, we respectively express the DGD and SOPMD in terms of the normalized quantities $\tau/\langle\tau\rangle$ and

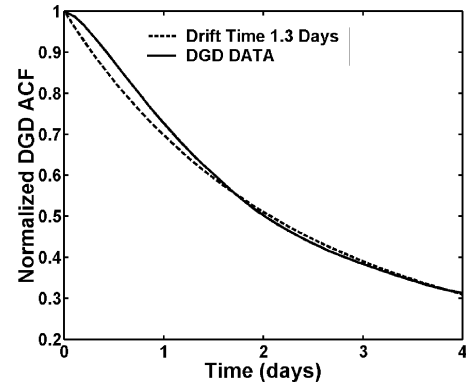


Fig. 2. Normalized wavelength-averaged temporal ACFs for the measured DGD (solid). The dashed theoretical fit corresponds to an average drift time of 1.3 days [6]. The SOPMD curves are similar.

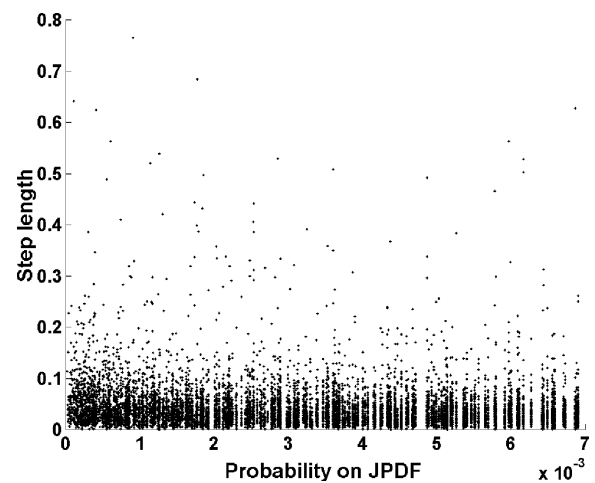


Fig. 3. Experimentally observed magnitude of the PMD state change ρ over one time step as a function of initial position on the J-PDF, indicating that the step size is independent of the initial PMD state.

$\tau_\omega/\langle\tau\rangle^2$, which will also serve, for example, as the horizontal and vertical axes in our graphs of the J-PDF. In particular, although the DGD and the SOPMD have differing dimensions, in the normalized J-PDF plane, we can define a dimensionless radius (i.e., step size) $\rho = (\Delta\text{DGD}^2 + \Delta\text{SOPMD}^2)^{1/2}$, of the change in the normalized PMD state (ΔDGD , ΔSOPMD) over a given time interval. This 2-D generalization of the normalized time step can be applied to a random walk over the J-PDF [2], [5]. Indeed, the experimentally measured distribution of the step sizes ρ as a function of the initial PMD states grouped according to their relative probability of occurrence (cf. Fig. 3) is approximately independent of the probability of the initial normalized (DGD and SOPMD) state. That is, the magnitude ρ of the variation in a PMD state over a time step depends negligibly on its location on the J-PDF.

To determine the distribution of ρ experimentally, we measured the temporal evolution of DGD and SOPMD in our fiber link. A histogram was constructed from all uncorrelated sets of fiber measurement data with a 1.6-h sampling period. The results, after linearly scaling to 1-h intervals, are shown in Fig. 4. To confirm that 1 h is sufficiently small compared to the PMD autocorrelation period, we created histograms from every

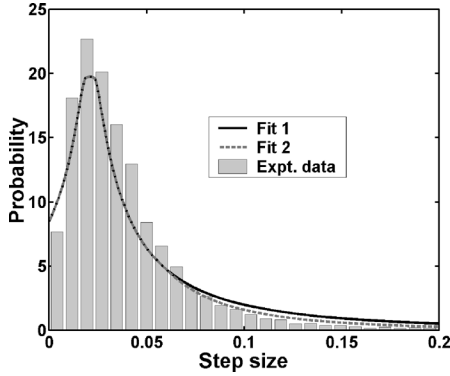


Fig. 4. Experimentally determined distribution of the normalized step size ρ for 1-h observation intervals for a 36-ps mean fiber. Two fits to the data are included that provide a self-consistency test of our empirical random-walk model. The step size is defined by the change in the PMD state on the normalized J-PDF.

second and third data point (corresponding to sampling at 3.2- or 4.8-h intervals, respectively). All three time intervals, i.e., 1, 3.2, and 4.8 h, resulted in identical histograms for ρ , implying that the estimated J-PDF does not depend on our sampling interval, which was far smaller than the correlation period. The step-size histogram displays a maximum near 0.025-scaled units. Large changes in the step size occur rarely and appear to be underestimated as a result of insufficient statistics.

To improve the computation efficiency of our subsequent calculations, we adopt the approximation

$$R(x) \approx \left(\frac{x - c_0}{c_1} \right)^2 \exp \left(- \frac{|x - c_0|^{c_2}}{c_3} \right) \quad (2)$$

to the experimentally measured PDF of Fig. 4, in which the values of c_n are determined through a nonlinear least squares fitting procedure. To avoid the zero in (2) at $x = c_0$ a second-order polynomial fit to the data was employed in the vicinity of this point. Our curve marked fit 1 was obtained with $c_0 = 0.021$, $c_1 = 5.94 \times 10^{-7}$, $c_2 = 0.15$, and $c_3 = 0.03$. These values were subsequently employed in the empirical random-walk simulations of outage durations. “Fit 2” is identical to fit 1 below a normalized step size of 0.06 but more accurately reproduces the measured step size distribution in the tail region. This second fit will be employed to establish the sensitivity of the empirical random-walk model to variations in least squares coefficients. Alternatively, although not implemented in this paper, a Metropolis sampling procedure can be employed to generate samples directly from the experimental step-size distribution.

IV. NUMERICAL MODELS OF PMD EVOLUTION

A. Empirical Random-Walk Model

We have shown that the magnitude of the change in PMD state is approximately independent of the initial position on the J-PDF. To further examine the direction of the PMD change at different location within the J-PDF, we employ a numerical technique for modeling time-dependent effects and DGD-induced outage rates that we term the “empirical” PMD evolution model. Here we generalize the observation of [2] that the probability distributions of the DGD as well as its rate of change

(in units of ps per hour) are uncorrelated to the temporal evolution of both the DGD and the SOPMD [2]. We observe that the change in the PMD state over a time step becomes more biased toward the higher probability central region of the J-PDF as the distance of the initial state from the maximum J-PDF value increases. Therefore, the direction of the change in PMD varies with position across the J-PDF space, while the magnitude of PMD change is independent of position on the J-PDF. Our empirical model calculation commences at an arbitrary point $P = (\text{DGD}, \text{SOPMD})$ on the normalized J-PDF (repeated simulations demonstrated that this result is independent of the initial value of P). A step size drawn from R is chosen as described above from a random distribution that is fit to the experimentally measured distribution of step sizes (Fig. 4) and a circle of this radius is drawn about P . The J-PDF is evaluated on the perimeter of this circle, and the step direction is selected from a random variable that is weighted according to the J-PDF values on the circle, yielding a new point P_1 . In this manner, the PMD change is preferentially directed towards higher probability regions of the J-PDF. We enhanced the computational efficiency without significantly affecting our results by sampling the “weighted circle” every 11.25° and discretizing the J-PDF on a grid of 400×500 points.

Repeating the above steps yields a random walk over the J-PDF. A system outage is recorded each time that the random walk crosses the outage boundary for the transponder (e.g., Fig. 1). However, since our calculations are performed in normalized PMD space, the outage boundary determined for an actual transponder must be expressed in dimensionless DGD and SOPMD units. For the receiver in Fig. 1, the boundary is a line from (45 ps, 0 ps²) through (40 ps, 2000 ps²). On the normalized J-PDF, this outage boundary transforms to a line from (1.8, 0) through (1.6, 3.2) for a $\langle \tau \rangle = 25$ ps fiber while for a $\langle \tau \rangle = 15$ ps fiber the line extends from (3.0, 0) to (2.67, 8.89). The duration of an outage then corresponds to the number of random-walk steps over which the PMD remains beyond the outage boundary. The frequency of outages is similarly given by the number of steps between successive outages. After a sufficient number of recorded outage events, we generate histograms of both the outage frequency and the duration. We have further verified that if this random-walk procedure is applied only to the DGD variable the resulting outage rates and durations agree with the integral method of [2] independent of the starting location P .

Comparing in Fig. 5 the PDFs formed from the histogram of visited states during the resulting random walk to the theoretical DGD and SOPMD distributions [5] yields a self-consistency test for the fitting procedure represented by (2). The simulated and expected distributions only diverge noticeably in the tail region (cf. Fig. 5) as the J-PDF distribution generated by the random walk, especially for improbable large step sizes, is noticeably affected by the step size distribution. Clearly fit 2 severely underestimates the tail of the PDF [Fig. 5(a)] while fit 1 more closely approximates the expected theoretical distributions of both the DGD and the SOPMD. Accordingly, while we employ fit 1 in the calculations of Section V, our calculation clearly establishes the importance of an accurate model of the step-size distribution R . Finally, under the assumption that

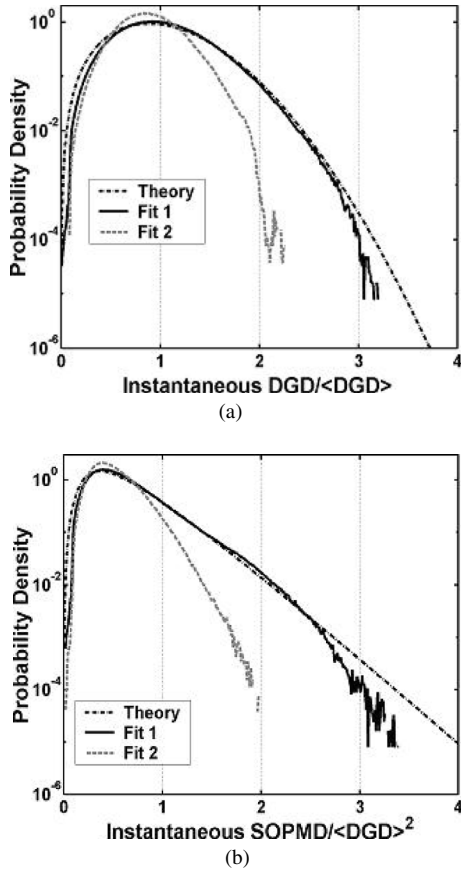


Fig. 5. (a) Probability density function of the DGD from the empirical model random-walk plotted against the known probability distributions for two choices of step sizes. The results obtained from fit 2 (dashed) underestimate the frequency of large DGD or SOPMD events, while those of fit 1 (solid) reproduce more accurately the theoretical distribution of DGD and SOPMD (dotted–dashed). (b) Same as Fig. 5(a) except for the PDF of the SOPMD.

our step size is representative of buried fibers that are exposed to similar environmental and/or mechanical conditions, our 2-D random-walk model should accurately predict outage probabilities as a function of the mean fiber DGD.

B. Fiber-Emulator Model

To provide a simple alternative to the empirical random-walk model discussed above, we calculated the frequency and duration of system outages directly from a fiber emulator model in which the change in the normalized DGD and SOPMD is recorded after random perturbations of the emulator angles that can be associated with the changes to the fiber properties over a time step. In our implementation, the relative orientation of the birefringence axes between two adjacent sections is specified by three angles describing rotations around fixed x , y , and z axes on the Poincaré sphere. The random change in these angles that is assumed to result from a single time step is simulated by adding randomly uniformly distributed values within $[-\theta_{\max}, \theta_{\max}]$ to the current angle. For consistency with Section IV-A, θ_{\max} is determined by comparing the numerically generated distributions of the step size ρ with experimental measurements. To obtain the optimum maximum perturbation angle $\theta_{\max} = 1.6^\circ$ employed in our calculations, we compared the simulated distribution for ρ from a 20-section fiber emulator for several values of θ_{\max} in

the range $0^\circ \leq \theta_{\max} \leq 3^\circ$ to the measured temporal evolution of the DGD and the SOMPD of Fig. 4.

We have further observed that the ACF of the PMD vector between the outputs of the fiber emulator after n and $n + k$ random perturbations of the mode-coupling angles (time steps) is described by

$$\left\langle \vec{\Omega}(n) \cdot \vec{\Omega}(n+k) \right\rangle \propto \frac{1 - \exp\left(-\frac{|k|}{n_d}\right)}{\left(\frac{|k|}{n_d}\right)} \quad (3)$$

in agreement with [6] in which the birefringence of each emulator segment rather than the coupling angles between adjacent segments varies randomly. The emulator’s “drift time” n_d is a measure of the average number of random perturbations required for the emulator to reach a PMD state that is decorrelated from the initial state. Since we have found numerically that $n_d \propto \theta_{\max}^2$ if all fiber sections are subjected to the same randomly fluctuating environment, the PMD time evolution can be simply and accurately modeled by equating n_d to the measured drift time of an installed fiber [13].

Associating each random perturbation of the fiber emulator with the 1-h sampling interval characteristic of the experimental measurement yields a predicted DGD autocorrelation time of 1.7 days, comparable to the measured value of 1.3 days from Fig. 2. Further, in Fig. 6(a) and (b), we verify numerically that the ρ obtained from a fiber emulator is nearly uncorrelated with the instantaneous value of DGD and SOPMD. In this and our subsequent fiber-emulator-based computations, we evenly distributed 70×70 histogram bins over the normalized region 0 to 3.5 in both the normalized DGD and the SOPMD. Fig. 6(a) then displays the distribution of the variation in the DGD and the SOPMD after a single time step ρ graphed as a function of the DGD of the initial state, calculated from 10^6 realizations of a 20-section fiber emulator. Similarly, the average magnitude of ρ across the DGD-SOPMD plane is plotted as a function of the coordinates of the initial state in the J-PDF of Fig. 6(b). While the mean value of ρ changes moderately with initial position in Fig. 6(b), this variation is several orders of magnitude less than the corresponding variation of the probability of the initial state. Therefore, we conclude that the numerically calculated distribution of ρ remains approximately constant over the J-PDF, consistent with the experimental observation of Fig. 3.

Finally, the frequency and duration of outage events were obtained from the fiber emulator model with a rapid transition matrix procedure for dynamic system modeling that was first introduced in [13]. Quantities such as the probability that a system with a particular initial value of the DGD will evolve into an outage event as a function of time are then simply evaluated [13].

V. RESULTS

From the outage boundary, Fig. 1, of a commercial 10-Gb/s transponder together with 6×10^6 emulator time steps (the equivalent of 700 years of PMD evolution within the framework of buried fiber temporal dynamics considered in this paper), we calculated the outage statistics associated with each of the

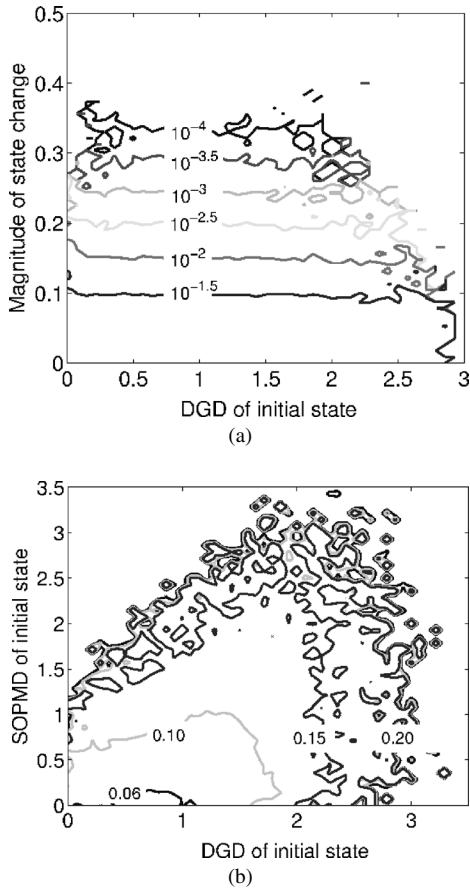


Fig. 6. (a) Magnitude of the change in the position in the DGD-SOPMD plane ρ of a state over one time step, graphed as a function of initial state as calculated with 10^6 realizations of a 20-section fiber emulator. (b) Contour map showing the average magnitude of the change in the position in the DGD-SOPMD plane ρ of a state over one time step plotted as a function of the coordinates of the initial state as calculated with 10^6 realizations of a 20-section fiber emulator.

numerical models of Section IV. We subsequently linearly normalized our results to correspond to a 20-year period.

Histograms for the outage duration and the period between outages for a fiber with 25-ps mean PMD are shown in Fig. 7(a) and (b) for the empirical random-walk model. Our model predicts that for this particular transponder deployed on a $\langle\tau\rangle = 25$ ps fiber, PMD outages occur an average of 38 times per year with mean and median outage durations of 10 and 4.8 h, respectively. Since the distribution of outages possesses a long tail with outage durations ranging from 4 min to 6.7 days, we believe that the median is the appropriate statistic in this context.

We verified the results of our empirical random-walk model by characterizing the outage performance of our measured OC-192 transponders on an installed fiber link. A 1 + 1 bidirectional OC-192 system was provisioned on a 3-span 110-km route of buried fibers with net $\langle\tau\rangle = 25$ ps. These fibers were in the same cable as the $\langle\tau\rangle = 36$ ps fiber of Fig. 4. Even though the fibers are different, we assume that the same step sizes can be employed in our model for different fibers exposed to the same environmental conditions [9]. The commercial transponders at the transmit and receive sides of the link were of identical design to those of Fig. 1 and

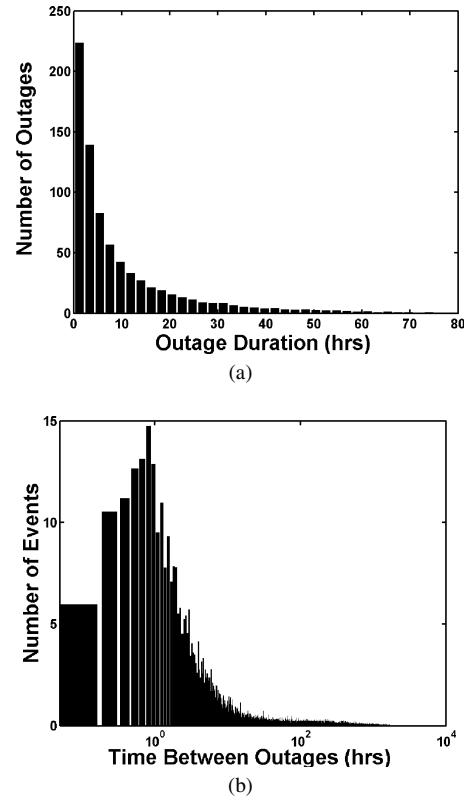


Fig. 7. (a) Histograms of the outage event durations for a 25-ps mean PMD fiber with the empirical random-walk model scaled to a 20-year time period with “fit 1” of Fig. 3. (b) Time between outages for the conditions described in Fig. 7(a).

accordingly exhibited similar performance sensitivity to DGD and SOPMD [7]. Chirped NRZ was transmitted through the amplifiers at each span termination to the receiver after which the BER performance was characterized from the raw SONET data stream. Over a 25-day period, the link experienced PMD outage events in three separate instances; day 2, day 12, and day 17, or roughly once every 8.3 days. In comparison, our outage simulation for a $\langle\tau\rangle = 25$ ps fiber for this receiver suggests an outage state every 9.6 days. Although the duration of the field trial was insufficient to yield statistically precise outage frequency and duration, the approximate agreement between simulation and measurement is encouraging.

The PMD tolerance is sensitive to factors such as the transponder design and the modulation scheme [7]. Therefore, to calculate network outages with our methods, the transmitter/receiver PMD tolerance and associated outage boundary for a given transponder must be independently determined. Once these values have been measured, however, the distribution of outage durations for fibers with differing mean DGD but equivalent temporal behavior can be immediately calculated. Our results for the number of outages per year and the median outage duration for fibers with mean DGD $15 \leq \langle\tau\rangle \leq 35$ ps are shown in Fig. 8(a) and (b). Here the J-PDF was not, however, obtained analytically but was instead generated by a Monte Carlo simulation with 10^9 fiber realizations in which the fiber was modeled as a concatenation of 2000 linearly birefringent sections. As a result, the J-PDF is not well defined beyond the 1.5×10^{-6} probability contour. The decreased

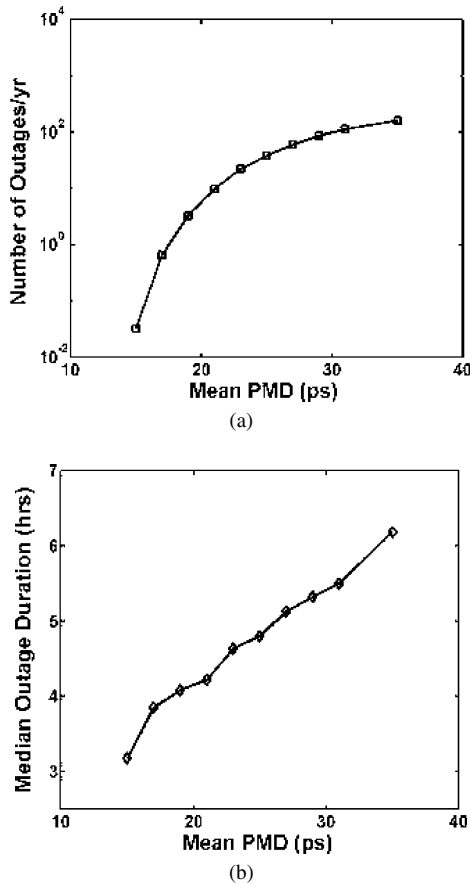


Fig. 8. (a) Expected number of outages per year for fibers with mean PMD from 15 to 35 ps with the empirical random-walk model for the step size distribution of fit 1 in Fig. 4. (b) Median outage duration for the conditions described in Fig. 8(a).

accuracy of the low-probability contours degrades the accuracy of our interpolation of the weighted circle at PMD states on the edge of the J-PDF, which typically results in an underestimate of the number of outages and their duration. We have found that for fibers with $\langle \tau \rangle > 17$ ps, the interpolation error has a negligible effect since most outages result from traversing regions where the J-PDF is well defined. However, for fibers with $\langle \tau \rangle < 17$ ps, the scaled outage boundary is at the extreme right of the J-PDF [e.g., (3.0, 0) through (2.67, 8.89) for a 15-ps mean fiber] and a significant fraction of the outages occur from walks that intersect the poorly defined region of the J-PDF. While the interpolation error can be minimized for moderate values of $\langle \tau \rangle$ through improved sampling techniques [14], [15], this source of numerical error can be eliminated by employing the analytic J-PDF [16] for small values of $\langle \tau \rangle$.

The fiber-emulator model of Section IV-B, on the other hand, yields results for the mean outage times with an outage boundary of 45 ps (cf. Fig. 9) that are not degraded by interpolation error. The corresponding curve for the mean number of outages per year in Fig. 9 agrees qualitatively with those of the previous figure but can be extended over many additional orders of magnitude (an analogous calculation of outage duration distributions is presented in [13]). Clearly, precise quantitative agreement is precluded by the different time-step distributions. With appropriate inputs, however, our method can be applied

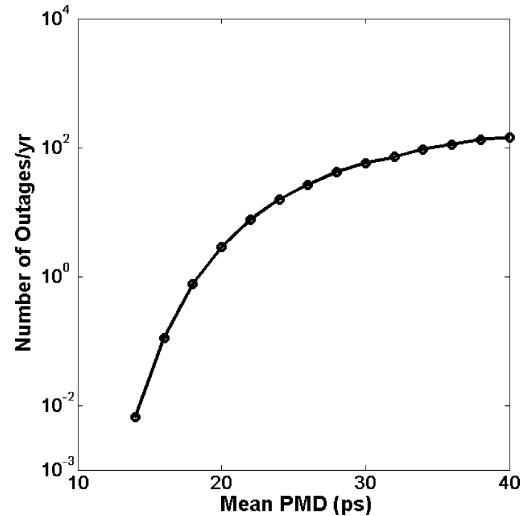


Fig. 9. Expected number of outages per year calculated with our numerical fiber emulator model for values of the mean PMD ranging from 14 to 40 ps and an outage boundary defined by a DGD of 45 ps.

to any transponder with known PMD tolerance, including 40- and 100-Gb/s systems.

VI. SUMMARY AND CONCLUSION

We have analyzed the effect of PMD on system performance over time with two novel random-walk models in conjunction with the probability distributions derived from PMD measurements of installed fibers. Our methods employ data from relatively short measurements of temporal PMD changes to predict system behavior at much later times, based on accurate models of both DGD and SOPMD effects. We determined that the step size of the PMD change is nearly independent of the magnitude of the PMD of a state. Moreover, the step sizes for the buried fiber characterized in this paper were small compared to the magnitude of the DGD and the SOPMD. Of course, longer term environmental changes such as seasonal changes are not registered unless, for example, the DGD and SOPMD measurements are repeated during the course of a year.

The system degradation resulting from PMD was measured by employing a programmable PMD source to define thresholds for outages for a specific fiber optic transponder. Running a random-walk model with these thresholds provided statistics that described the quantity and duration of PMD-induced outages over time. The distribution of the visited DGD and SOPMD states over the random-walk was then compared with theory, providing a self-consistent check of our results. This procedure not only ensures that the PMD evolution follows theoretically expected distributions but also leads to an interesting speculation. Our simulations indicate that precise agreement between the expected PDF of the DGD and SOPMD and that obtained from the random-walk procedure requires an accurate model of the step-size distribution R . If, however, only the correct scaling of R is required to produce an adequate agreement, the temporal fiber measurement procedure could possibly be further simplified, providing new insight into PMD-induced outages.

Our techniques enable the analysis of rare outage events caused by PMD, as well as of variations of receiver perfor-

mance resulting from DGD and SOPMD. Through appropriate scaling, they can be applied to an entire class of fibers with certain similar characteristics that are subjected to dynamic environments. Our methods can also be employed to characterize receivers and PMD compensators and to calculate service availability in the presence of a wide class of time-dependent sources of pulse distortions.

Finally, we have applied, to our knowledge for the first time, our recently advanced transition matrix analysis to an experimental problem. The results of these calculations further justify our simplified empirical model for time-dependent effects.

REFERENCES

- [1] H. Kogelnik and R. M. Jopson, "Polarization-mode dispersion," in *Optical Fiber Telecommunications*, I. Kaminow and T. Li, Eds. New York: Academic, 2002, vol. IVB, p. 788.
- [2] R. Caponi, B. Ripoati, A. Rossaro, and M. Schiano, "WDM design issues with highly correlated PMD spectra of buried optical cables," in *Proc. Opt. Fiber Commun. Conf.*, Anaheim, CA, 2002, pp. 453–455, Th15.
- [3] A. Papoulis, *Probability, Random Variables, and Stochastic Processes*, 3rd ed. New York: McGraw-Hill, 1991.
- [4] C. Antonelli, A. Mecozzi, M. Brodsky, and M. Boroditsky, "A simple analytical model for PMD temporal evolution," in *Proc. Opt. Fiber Commun. Conf.*, Anaheim, CA, 2002, OwJ4.
- [5] G. J. Foschini, L. E. Nelson, R. M. Jopson, and H. Kogelnik, "Probability densities of second-order polarization mode dispersion including polarization dependent chromatic fiber dispersion," *IEEE Photon. Technol. Lett.*, vol. 12, no. 3, pp. 293–295, Mar. 2000.
- [6] M. Karlsson, J. Brentel, and P. Andrekson, "Long-term measurement of PMD and polarization drift in installed fibers," *J. Lightw. Technol.*, vol. 18, no. 7, pp. 941–951, Jul. 2000.
- [7] H. H. Yaffe and D. L. Peterson Jr., "Experimental determination of system outage probability due to first and second order PMD," *J. Lightw. Technol.*, vol. 24, no. 11, pp. 4155–4161, Nov. 2006.
- [8] J. N. Damask, G. J. Simer, K. B. Rochford, and P. R. Myers, "Demonstration of a programmable PMD source," *IEEE Photon. Technol. Lett.*, vol. 15, no. 2, pp. 296–298, Feb. 2003.
- [9] D. L. Peterson, B. C. Ward, K. B. Rochford, P. J. Leo, and G. Simer, "Polarization mode dispersion compensator field trial and field fiber characterization," *Opt. Express*, vol. 10, pp. 614–621, 2002.
- [10] B. L. Heffner, "Automated measurement of polarization mode dispersion using Jones matrix eigenanalysis," *IEEE Photon. Technol. Lett.*, vol. 4, no. 9, pp. 1066–1069, Sep. 1992.
- [11] M. Karlsson and J. Brentel, "Autocorrelation function of the polarization-mode dispersion vector," *Opt. Lett.*, vol. 24, pp. 939–941, 1999.
- [12] M. Shtaif and A. Mecozzi, "Study of the frequency autocorrelation of the differential group delay in fibers with polarization mode dispersion," *Opt. Lett.*, vol. 25, pp. 707–709, 2000.
- [13] D. Yevick and M. Reimer, "Transition matrix analysis of system outages," *IEEE Photon. Technol. Lett.*, vol. 19, no. 19, pp. 1529–1531, Oct. 2007.
- [14] D. Yevick, "Multicanonical evaluation of joint probability density functions in communication system modeling," *IEEE Photon. Technol. Lett.*, vol. 15, no. 11, pp. 1540–1542, Nov. 2003.
- [15] D. Yevick, "Multicanonical communication system modeling—Application to PMD statistics," *IEEE Photon. Technol. Lett.*, vol. 14, no. 11, pp. 1512–1514, Nov. 2002.
- [16] E. Forestieri, "A fast and accurate method for evaluating joint second-order PMD statistics," *J. Lightw. Technol.*, vol. 21, no. 11, pp. 2942–2952, Nov. 2003.

D. Yevick, (SM'86–F'96) photograph and biography not available at the time of publication.

M. Reimer received the B.Sc. degree in honors physics (co-op) from the University of British Columbia, Vancouver, BC, Canada, in 1999 and the M.Sc. degree in applied physics from the University of Waterloo, Waterloo, ON, Canada, in 2007, where he is currently working towards the Ph.D. degree in applied physics under the supervision of Prof. D. Yevick.

Before 2005, he was with the next generation optical network design team at Nortel Networks.

Mr. Reimer received the Outstanding Achievement in Graduate Studies distinction from the University of Waterloo for top academic standing at the graduate level in the Faculty of Science and holds the Alexander Graham Bell Canada Graduate Scholarship (Doctoral) from the Natural Science and Engineering Research Council of Canada (NSERC).



H. Yaffe (M'03) received the B.A. degree from Swarthmore College, Swarthmore, PA, and the M.Sc. and Ph.D. degrees in applied physics from Weizmann Institute of Science, Rehovot, Israel.

He is the President of New Ridge Technologies, LLC, Reisterstown, MD, where he oversees the day-to-day operation of the company. Before New Ridge, Yaffe was the founder of YAFO Networks, where he led the development of the first network qualified PMD compensator and associated technologies. Prior to YAFO, he had various responsibilities for network systems and optical technologies at CIENA. He has also held technical positions with Bell Laboratories in Murray Hill, NJ and Norcross, GA focusing in planar waveguide technology and projection CRTs. He has authored numerous academic publications and conference presentations and he is an inventor of 15 patents.

P. J. Leo, photograph and biography not available at the time of publication.

D. L. Peterson, (S'91–M'91–SM'04) photograph and biography not available at the time of publication.

S. Wang, photograph and biography not available at the time of publication.

K. B. Rochford, (S'89–M'90–SM'01) photograph and biography not available at the time of publication.